The properties of Al doped ZnO thin films deposited on various substrate materials by RF magnetron sputtering

Xiaojin Wang · Xiangbin Zeng · Diqiu Huang ·
Xiao Zhang · Qing Li

Abstract Transparent conductive Al-doped ZnO (AZO) thin films were deposited on various substrates including glass, polyimide film (PI) and stainless steel, using radio frequency magnetron sputtering method. The structural, electrical and optical properties of AZO thin films grown on various substrates were systematically investigated. We observe that substrate materials play important roles in film crystallization and resistivity but little on optical transmittance. X-ray diffractometer study shows that all obtained AZO thin films have wurtzite phase with highly c-axis preferred orientation, and films on glass present the strongest (002) diffraction peaks. The presence of compression stress plays critical role in determining the crystalline structure of AZO films, which tends to stretch the lattice constant c and enlarge the (002) diffraction angle. Although the films on the glass present the finest electrical properties and the resistivity reaches 12.52×10^{-4} Ωm, AFM study manifests that films on flexible substrates, especially stainless steel, bestrew similar inverted pyramid structure which are suitable for window material and electrode of solar cells. The average optical transmittance of AZO thin films deposited on glass and PI are both around 85% in the visible light range (400–800 nm).

1 Introduction

Low electrical resistivity and high optical transmittance have made transparent conducting oxides (TCO) such as tin-doped In_2O_3 (ITO), SnO_2 been widely used in practical applications as flat-panel displays, transparent electrodes, opto-electronic devices and photovoltaic cells [1]. Currently, the In_2O_3 films such as tin-doped In_2O_3 (ITO), SnO_2:Sb (ATO) and SnO_2:F (FTO) have been extensively used in practical applications [2]. However, the In_2O_3 films own many inherent defects: (1) In and Sn are scarce nonrenewable resources, thus the cost is expensive; (2) The chemical property of In and Sn are lively, which is unstable at the hydrogen plasma atmosphere in fabricating various devices; (3) The relatively high atomic weight of In and Sn which tends to poison substrate materials, especially for the silicon-based solar cells and liquid crystal displays [3–9]. AZO is a potential substitute for ITO in corresponding applications because it is low-cost and non-toxic as well as good stability in the present of hydrogen plasma [10–14]. Moreover, a comparison with ITO shows that AZO fims can be prepared by various fabrication techniques [15] at low temperature and have good electrical conductivity and optical transmittance [16].

Up to now, a number of studies on AZO films deposited on various substrates have been carried out [17–21]; however, most attention was paid to the influence of deposition conditions on the properties of AZO films rather than substrate selection. Properties of epitaxial growth AZO thin film rely on substrate properties such as crystal orientation, surface topography, stability as well as inherent performance. In this paper, we have chosen glass and two typical flexible materials (PI film and stainless steel) as substrates because much attention has been paid to replace glass with flexible substrates in thin film solar cells and flat-panel display technologies. We deposited AZO films on glass, PI and stainless steel by radio frequency (RF) magnetron sputtering method under the same conditions. In order to give an in-depth research on the dependence of AZO films

X. Wang · X. Zeng (✉) · D. Huang · X. Zhang · Q. Li
Department of Electronic Science and Technology, Huazhong University of Science and Technology, Wuhan 430074, Hubei, People's Republic China
e-mail: eexbzeng@163.com

properties on substrate materials, a comparison of the properties for AZO films on various substrates is given.

2 Experimental details

AZO thin films were deposited on glass, PI and stainless steel under the same deposition conditions using RF magnetron sputtering. All substrates were carefully cleaned in acetone, rinsed in alcohol and then cleaned in an ultra-sonic cleaner within DI water. The sintered ceramic ZnO disk containing 2 wt% Al_2O_3 with a diameter of 60 mm was used as sputtering target. The substrates were placed parallel to the target surface with a 60 mm distance. The deposition duration was fixed at 2 h. Pure argon gas was introduced into the chamber at a base pressure of 10^{-4} Pa. The argon flow rate was constant 20 sccm, which was controlled by mass flow controller, and the deposition pressure was 1 Pa. The sputtering RF power was controlled at 120 W for the 14.13 cm^2 target surface. The substrate temperature was fixed at 300 °C.

X-ray measurements were carried out at room temperature (25 °C) on an X-ray diffractometer (XRD, X'Pert PRO). All the available reflections were recorded for AZO films from an angle 2θ of 10–90° and the step size [2θ] is 0.0170°, using high intensity (40 kV and 40 mA) filtered Cu_α radiation. The alignment of the diffractometer was verified by a silicon sample. The surface morphologies were observed using atomic force microscope (AFM) under contact mode as well as field scanning electron microscopy (FE-SEM). Resistivity, carrier concentration and Hall mobility of the AZO films were measured by using Hall measurement system (Lakeshore MODEL 642). The optical transmittance was measured by UV visible spectrophotometer (UV-2550) in the wavelength of 300–900 nm. Film thickness was measured by the traditional α-step method (KLA TENCOR P16+).

3 Results and discussion

3.1 Structure properties

Figure 1 shows XRD patterns of AZO thin films deposited on glass (a), PI film (b) and stainless steel (c), respectively. Compared the XRD pattern of AZO film on stainless steel with that on glass and PI, there are three surplus peaks (S) locating at 43°, 50° and 74°. In order to explain it, we examined the XRD spectra of the stainless steel substrate. In Fig. 1d, we can see that the surplus peaks are dominated by stainless steel rather than AZO films.
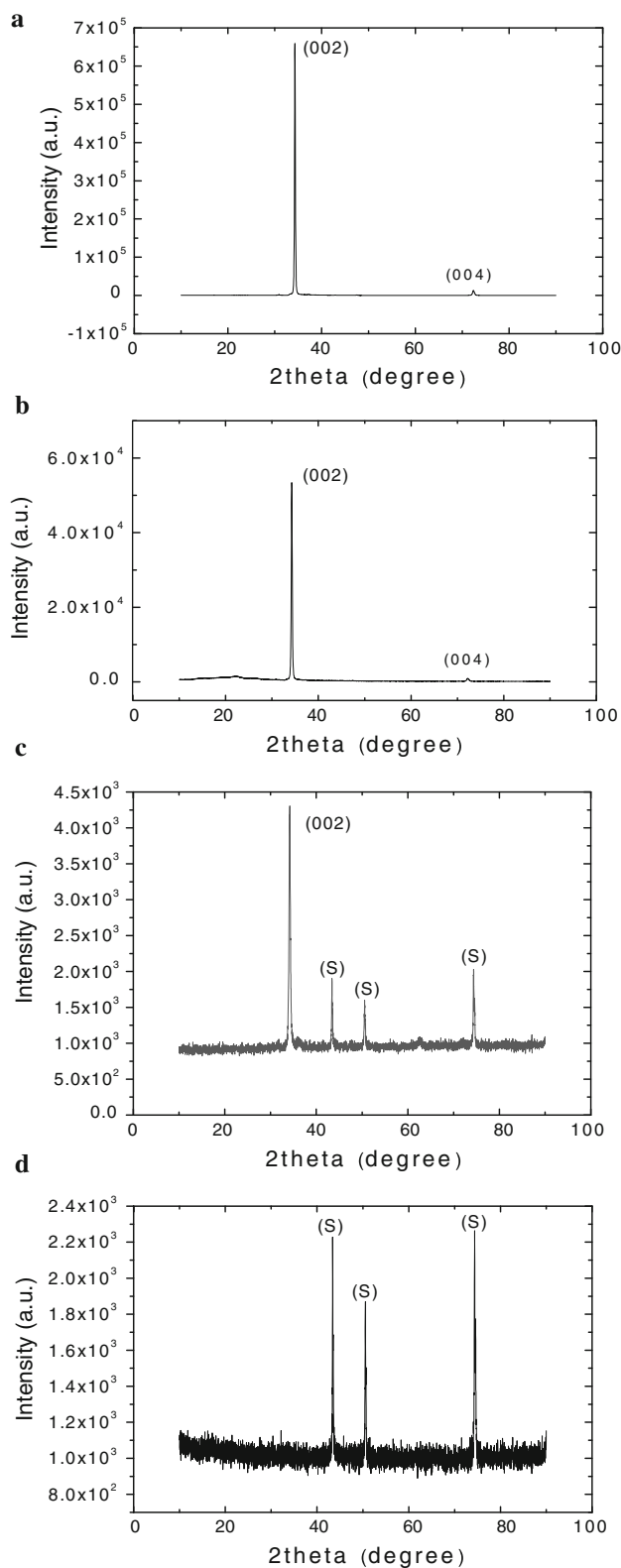

Fig. 1 XRD spectra of **a** AZO thin film deposited on glass, **b** AZO thin film deposited on PI substrate, **c** AZO thin film deposited on stainless steel, **d** stainless steel

Table 1 XRD data and crystal size of the AZO films deposited on glass, PI film and stainless steel

Substrate	2θ (°)	FWHM (°)	Crystal size (nm)	Intensity (a.u.)	Thickness (Å)
Glass	34.2804	0.1632	50.37341	641,448.30	6,462
PI film	34.2506	0.2007	40.95806	51,474.37	6,447
Stainless steel	34.2045	0.2509	32.75912	3,280.42	6,453

AZO films grown on glass substrates showed stronger and sharper (002) diffraction peak than AZO films on PI and stainless steel. The XRD diffraction intensity of AZO films deposited on PI and stainless steel was 51,474.37 and 3,280.42, respectively, much weaker than 641,448.30 on glass substrates. The FWHM of AZO films grown on glass, PI and stainless steel were 0.1632, 0.2007 and 0.2509°, respectively, is given in Table 1. Based on the above analysis, the films deposited on glass present the best crystallinity; nevertheless, AZO films on the flexible substrates, PI and stainless steel, also exhibit highly preferential c-axis orientation with good crystallinity. The (002) diffraction peaks of the AZO films deposited on glass, PI film and stainless steel are located at $2\theta = 34.2804°$, $2\theta = 34.2506°$ and 34.2045°. This means that AZO films deposited on flexible substrates have almost the same structure as those deposited on glass substrates. From the X-ray diffraction spectra, we observed that AZO films deposited on glass and PI exhibit another peak originated from (004) with much weaker intensity, which indicates both of them are polycrystalline with a hexagonal structure. While films on the stainless steel do not show such a diffraction peak, it is quite possible that a weak (004) peak is covered by the noise signal. From the analyses of the XRD data showed in Table 1, it is obvious that films on stainless steel have relatively poor crystallographic structure than films on glass and PI in terms of FWHM, crystal and diffraction intensity. Overall, substrate materials play decisive influence on the crystal properties but little on the lattice structure of the AZO films when the deposition conditions kept the same.

In order to analyze the influence of substrate materials on grain size, we evaluate the mean grain size (d) of AZO films. We adopted the Scherrer's equation [22]

$$d = 0.9 \frac{0.9\lambda}{B\cos(\theta)} \tag{1}$$

where λ, B and θ are X-ray wavelength (1.54060 Å), FWHM and Bragg diffraction angle, respectively. The calculated results and XRD data are indicated in Table 1. The average thickness of AZO films was approximately 6,450 Å, without considerable change with the substrate materials.

We can see that the crystal size of AZO films deposited on PI and stainless steel are 40.9586 and 32.75912 nm, much smaller than that of 50.37341 nm on glass substrates.

Table 2 The value of stress, constant c and 2θ for AZO films deposited on various substrates

Substrate	Glass	PI film	Stainless steel
Stress ($\times 10^9$ Nm^{-2})	−1.81	−2.19	−2.77
Constant c (Å)	5.1945	5.2017	5.2047
2θ (°)	34.2804	34.2506	34.2045

The discrepancy of grain size and crystalline structure can be illustrated by the presence of stress when the sputtering conditions kept the same. The illustration will be given afterwards.

For hexagonal lattice crystals, the linear components are given by [23]

$$\begin{pmatrix} \sigma_x \\ \sigma_y \\ \sigma_z \end{pmatrix} = \begin{pmatrix} C_{11} & C_{12} & C_{13} \\ C_{12} & C_{11} & C_{13} \\ C_{13} & C_{13} & C_{33} \end{pmatrix} \begin{pmatrix} e_{xx} \\ e_{yy} \\ e_{zz} \end{pmatrix}, \tag{2}$$

where C_{ij} are the elastic stiffness constants and e_{xx}, e_{yy} and e_{zz} are the linear strain in the x, y and z axis, respectively.

Hoffman [24] has shown that the stress σ_z is zero in films except very close to the edges. Thus, S. Maniv [23] has deduced that the stress in the plane of the film is

$$\sigma = [2C_{13} - C_{33}(C_{11} + C_{12})/C_{13}]e_{zz}, \tag{3}$$

And e_{zz} is the linear strain along the z axis, which can be calculated by

$$e_{zz} = \frac{c - c_0}{c_0}, \tag{4}$$

where c_0 is the lattice parameter of stress-free bulk ZnO, and c is the lattice constant obtained from the (002) planes in the XRD spectrum. The values of the elastic stiffness constant are $C_{11} = 2.1 \times 10^{11}$ Nm^{-2}, $C_{12} = 1.2 \times 10^{11}$ Nm^{-2}, $C_{13} = 1.05 \times 10^{11}$ Nm^{-2} and $C_{33} = 2.1 \times 10^{11}$ Nm^{-2}. Substituting these values and Eq. 4 in the Eq. 3, finally, the stress σ is obtained

$$\sigma = 4.5 \times 10^{11}(c - c_0)/c_0 \text{Nm}^{-2}. \tag{5}$$

The variation of stress σ with substrates is shown in the Table 2. The stress in the films ascribes to two main aspects. One is the intrinsic stress introduced by the doping and generating defects in the films, the other is the extrinsic stress introduced by mismatch of lattice and thermal expansion coefficients between substrate materials and

AZO films. Bhupensra K Sharma and Neeraj Khare [25] have reported that the change of stress in the AZO films is mainly from the doping amount of Al in the ZnO films when substrates and sputtering conditions are the same. In the present case, the substrates varied but the deposition conditions kept the same. So we attribute the variation of stresses to the change of substrate materials. Table 2, σ varies from -1.81×10^9 Nm^{-2} to -2.77×10^9 Nm^{-2} and becomes increasingly compressive. By contrast, the intensity of (002) diffraction peak shows downward trend, decreasing from 641,448.30 a.u. on glass to 3,280.42 a.u. on stainless steel. The variation of the diffraction intensity and crystalline structure can be illustrated by the effect of compressive stress. The stress existed in the films is likely to squeeze the lattice, consequently AZO films tend to achieve larger lattice constant c. The lattice constants c of AZO films on glass, PI and stainless steel are 5.1945, 5.2017 and 5.2047 Å, which are smaller than the $c_0 = 5.2066$ Å of stress-free bulk ZnO. Showed in Table 2, the constant c varies directly with the stress. According to the Bragg diffraction theory ($2d \sin\theta = n\lambda$), diffraction angle θ is inversely proportional to lattice constant c ($c = 2d$). Consequently, θ is inversely with the stress intensity and films with larger stress tend to acquire larger (002) diffraction angle. As showed in Table 2, 2θ decreases from 34.2804 on glass to 34.2506 on PI to 34.2045 on stainless steel.

On the other hand, the presence of stress is related to the film stoichiometry, the mismatch in the thermal expansion coefficients and lattice imperfections [26, 27]. However, the thermal expansion coefficients of glass and stainless steel are relatively small. Before we put the PI substrate into the sputtering chamber, the PI was pre-baked at 300 °C for 2 h till there were no gas molecules and steam evaporating from the PI substrate. By pre-baking process, we released the stress and mechanical coefficients in the PI material and minimized the influence of thermal expansion coefficients. Therefore, we mainly focused on the effect of lattice mismatch on the presence of stress.

3.2 Morphological characteristics

The dependence of crystallinity and crystal size on the substrate for the AZO films is further revealed by FESEM micrographs. Figure 2 shows the FESEM morphologies of AZO films deposited on various substrates. We can see that the grain distributions of AZO films are uniform with dense microstructure. It's evident that films on varied substrates showed different microscopic surface texture. Figure 2 shows the SEM microstructures of films on different substrate materials. Films on glass are dense and hill-shaped, distributing with lots of mountains. As to films on PI, the surface is spread with schistose structures and craters formed between the structures. However, films on the stainless steel are saturated with small granular grains and grain boundaries. Perhaps lattice and thermal expansion coefficients mismatch make the films grown on various substrates exhibit various microstructure and surface morphology.

Figure 3 shows AFM topographies of the AZO thin films deposited on three different substrates. The root mean square (RMS) average roughness of the AZO surface was calculated from a 2 μm × 2 μm rectangular scan area. The RMS average roughness of the AZO film grown on glass is 1.968 nm, smaller than that 2.252 nm on PI and 4.955 on stainless steel, which are showed in Table 3. AZO films are mainly used in solar cells as transparent electrodes and window materials, therefore appropriate surface roughness helps to reduce light reflection and increase optical path. Films on flexible substrates exhibit larger roughness than films on glass, which it is beneficial to light absorption and suitable for solar cells application. From AFM, we can see that films on flexible substrates are scattered with pyramid structures, especially films on stainless steels are saturated with similar inverted pyramid structures. A large number of nanometer-sized mountains formed on the surface of AZO films on stainless steel, as shown in Fig. 3c. Based on the morphological analysis, films deposited on flexible
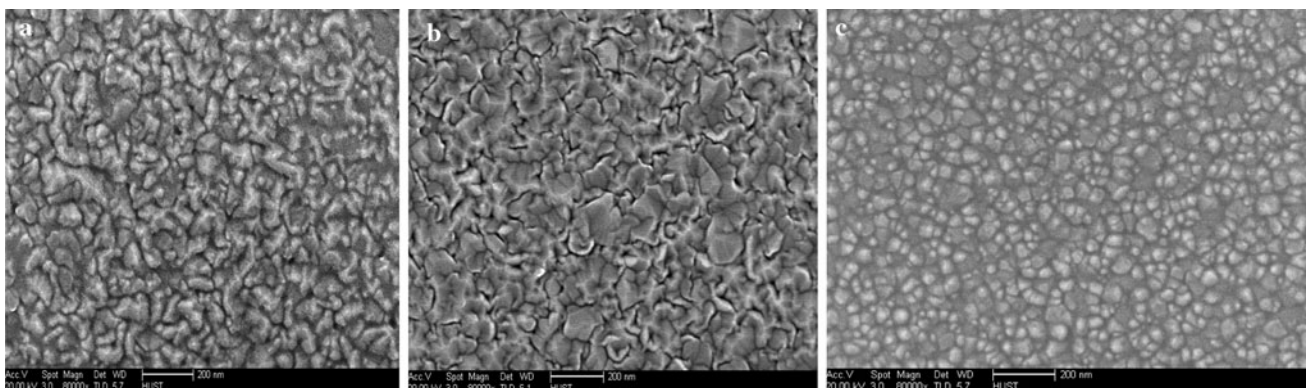

Fig. 2 SEM microstructures of AZO thin films deposited on a glass, b PI and c stainless steel
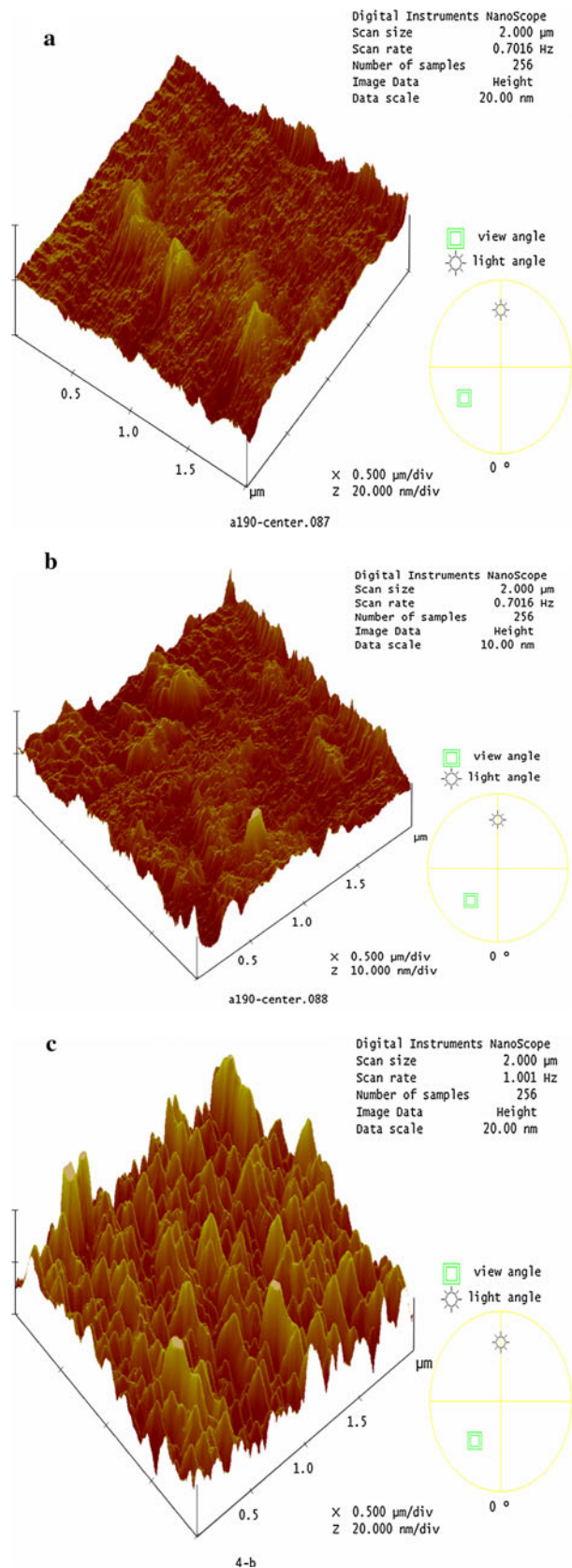
Fig. 3 AFM images of AZO thin films deposited on **a** glass, **b** PI film and **c** stainless steel

Table 3 Electrical properties and RMS average roughness of AZO films deposited on various substrates

Substrate materials	Glass	Pi film	Stainless steel
Resistivity ($\times 10^{-4}$ Ωcm)	2.352	6.336	1.252
Carrier concentration ($\times 10^{21}$ cm^{-3})	2.88	2.68	2.41
Hall mobility (cm^2/Vs)	9.73	4.14	2.46
Roughness (nm)	1.968	2.252	4.955

substrates are more suitable for window materials and top electrodes in solar cells.

3.3 Electrical properties

The electrical properties of AZO thin films deposited on various substrates were investigated by a Hall measurement system. Table 3 shows the electrical properties of AZO thin films as a function of substrate materials.

It has been known that various scattering mechanisms might be involved in semiconductor materials, including ionized impurity scattering, neutral impurity scattering and grain-boundary scattering [27]. When the deposition conditions kept the same and varied the substrate materials, the electrical properties are mainly affected by grain-boundary scattering.

As shown in Table 3, the resistivity of AZO films varied with the substrate materials. The minimum resistivity 2.352×10^{-4} Ωcm is obtained from AZO films deposited on glass substrates. The electrical property is a little worse on flexible substrates with the resistivity 6.336×10^{-4} Ωcm on PI and 1.252×10^{-3} Ωcm on stainless steel. The electrical resistivities of the films decreased gradually with the increase of crystallite size and the improvement of crystallinity for the AZO films, which has been confirmed by D. Zhu et al. [28, 29]. The increase of crystallite size and the improvement of crystallinity will lead to the decrease of grain boundaries, reducing the abilities of scattering and capturing current carriers. AZO films on the stainless steel Fig. 2c are saturated with small granular grains, generating lots of grain boundaries. Thus degrade the electrical performance. By contrast, films on glass and PI owned larger grain size and better crystallinity, so AZO films on glass and PI presented relatively low resistivity.

Also it was found that the resistivity decrease showed in Table 3 was related to decrease of both Hall mobility and carrier concentration. It also interpreted as carrier transport dominated by grain boundary scattering resulting from trapping of free electrons due to oxygen adsorption on the grain boundary surface because the free electron trapping results in a simultaneous decrease of both carrier concentration and mobility due to an increase of potential barrier

height at the grain boundary [30]. So, films with fewer boundaries present better electrical properties. As can be seen AZO films on glass have largest grain size and least grain boundaries, followed by films on PI and stainless steel. Consequently, the carrier concentration decreased from 2.88×10^{21} cm^{-3} on glass to 2.68×10^{21} cm^{-3} on PI to 2.41×10^{21} cm^{-3} on stainless steel and Hall mobility decreased from 9.73 cm^2/Vs on glass to 4.14 cm^2/Vs on PI to 2.46 cm^2/Vs on stainless steel.

Although the resistivity of films on flexible substrates is not comparable to films on glass, we have fabricated low resistivity films on PI and stainless steel which are suitable for flexible solar cells.

3.4 Optical properties

The stainless steel substrate is opaque. Owing to limit of testing technique, we investigated the optical properties of the AZO thin films deposited on glass and PI substrates. Figure 4 shows the transmission spectra of AZO thin films deposited on glass and PI substrates. We can see that the average optical transmittance of the samples in the visible light range (400–800 nm) is both around 85%.

Research has confirmed that film thickness [31], amounts of Al$_2$O$_3$ [32] as well as film crystallinity [33] play decisive roles in optical transmittance. When the deposition conditions kept the same, films on various substrates have almost the same thickness (showed in Table 1) and amounts of Al$_2$O$_3$. Therefore, the variation of optical transmittance for films on various substrates is mainly determined by film crystallinity. According to the XRD analysis, the crystallinity of specimen was changed slightly. So the optical properties of AZO films were not changed considerable with substrate materials.
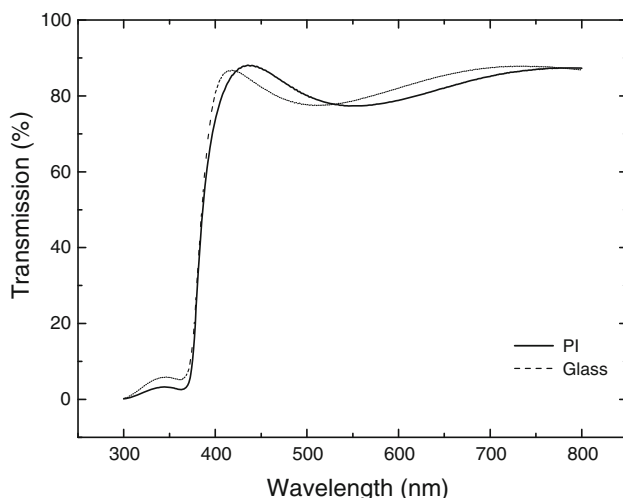
Overall, the optical transmittance of AZO films was not changed with substrates even though the crystallinity of the films with different substrates was changed.

4 Conclusions

Highly transparent conducting AZO thin films with low resistivity were deposited on glass, PI and stainless steel substrates by RF magnetron sputtering. A comparison of the optical, electrical and structure properties for films grown on different substrate materials was given. It was found that the substrate properties were critical factors for film crystallinity and resistivity, but little influence on optical transmittance.

Although the quality of the films deposited on PI and stainless steel substrates is somewhat worse than films on glass substrates, both of them have highly preferential c-axis orientation with good crystallinty. Films with good structure properties have resistivity as low as 6.336×10^{-4} Ωcm on PI substrates and 1.252×10^{-3} Ωcm on stainless steel substrates. Moreover, PI and stainless steel can be used as flexible substrates in preparing AZO thin films by magnetron sputtering, and films on the substrates present similarly inverted pyramid which are suitably used as top electrodes, buffer layers and window materials in flexible solar cells and plastic liquid crystal displays.

Fig. 4 Optical transmission spectra of AZO films deposited on glass and PI substrate

References

1. X. Jiang, F.L. Wong, M.K. Fung, S.T. Lee, Applied Physics Letters **83**(9), 1875–1877 (2003)
2. Zhaoquan, C., Minghai, L., Yuping, L., Peng, H., Liang, T., & Xiwei, H. *Proceedings of SPIE*, (vol 7518 75180X-1).
3. T. Minami, H. Nanto, S. Takata, Applied Physics Letters **41**, 958 (1982)
4. A.L. Dawar, J.C. Joshi, J. Mater, Science **19**, 1 (1984)
5. P. Song, M. Watanabe, M. Kon, A. Mitsui, Y. Shigesato, Thin Solid Films **411**, 82 (2002)
6. W.-J. Jeong, G.-C. Park, Sol. Energy Mater. Sol. Cells **65**, 37 (2001)
7. J. Hu, R.G. Gorden, Journal of Applied Physics **71**, 880 (1992)
8. X.-T. Hao et al., Materials Science and Engineering **B90**, 50–54 (2002)
9. B.-Y. Oh, M.-C. Jeong, T.-H. Moon, W. Lee, J.-M. Myoung, D.-S. Seo, Journal Applied Physics **99**(12), 124505-1-4 (2006)
10. T. Minami, K. Oohashi, S. Takata, Thin Solid Films **193**, 721 (1990)

11. K. Shin, K. Prabakar, W.-P. Tai, J.-H. Oh, C. Lee, Journal of the Korean Physical Society **45**, 1288 (2004)
12. O. Kappertz, R. Drese, M. Wuttig, Journal of Vacuum Science & Technology A **20**, 2084 (2002)
13. Y. Lgasaki, H. Saito, Journal of Applied Physics **69**, 2190 (1991)
14. M. Karger, M. Schiling, Physical Review B **71**, 075303 (2005)
15. Yang, Z., Zheng, H., Li, X., Peng, Y., Zhao, Q., & Liu, B. *Proceedings of SPIE* (vol 7655).
16. L. Lu et al., Physical Review B **405**, 3320–3323 (2010)
17. K. Shin, K. Prabakar, W.-P. Tai, J.-H. Oh, C. Lee, Journal of the Korean Physical Society **45**, 1288 (2004)
18. N.-H. Kim, H.-W. Kim, Materials Letters **58**, 938 (2003)
19. S.-K. Hong, T. Hanada, H. Ko, Y. Chen, T. Yao, D. Imai, K. Arak, M. Shinohara, K. Saitoh, M. Terauchi, Physical Review B **65**, 115331 (2002)
20. M.-Y. Han, J.-H. Jou, Thin Solid Films **260**, 58 (1995)
21. O. Kappertz, R. Dress, M. Wuttig, Journal of Vacuum Science & Technology A **20**, 2084 (2002)
22. M. Karger, *Thin film analysis by X-ray scattering* (Wiley-Vch Verlag Gmbh & Co, Kgaa, 2006), p. 110
23. S. Maniv, W.D. Westwood, E. Colombini, Journal of Vacuum Science & Technology **20**, 162 (1982)
24. D.W. Hoffmand, J.A. Thornton, Journal of Vacuum Science & Technology **17**, 743 (1980)
25. B.K. Sharma, N. Khare, J. Phys. D Appl. Phys. **43**, 465402 (2010)
26. N. Hasuike, H. Fukumura, H. Harima, K. Kisoda, H. Matsui, H. Saeki, H. Tabata, Journal of Physics, Condensed Matter **16**, S5807 (2004)
27. T. Minami, H. Nanto, S. Takata, Japanese of Applied Physics **23**, 280 (1984)
28. D. Zhu et al., Applied Surface Science **255**, 6145–6148 (2009)
29. V. Musat et al., Surface and Coatings Technology **180–181**, 659–662 (2004)
30. J. Nomoto et al., Journal of Vacuum Science & Technology A **28**, 4 (2010)
31. W.-J. Jeong, G.-C. Park, Sol. Energy Mater. Sol. Cells **65**, 37–45 (2001)
32. P. Kim, Ma, Journal of Applied Physics **81**(12), 15 (1997)
33. D.H. Kim et al., Applied Physics Letters **76**, 3 (2000)